Thin Solid Films, Volume 688, 31 October 2019, Article number 137358
DOI:10.1016/j.tsf.2019.06.008

Elevated temperature micro-impact testing of TiAlSiN coatings produced by physical vapour deposition

Ben D. Beake[1,*], Andrew Bird[1], Luis Isern[2], Jose L. Endrino[2] and Feng Jiang[3]

1 Micro Materials Ltd, Willow House, Yale Business Village, Ellice Way, Wrexham, LL13 7YL, UK

2 School of Aerospace, Transport and Manufacturing, Cranfield University, Bedford, MK43 0AL, UK

3 Institute of Manufacturing Engineering, Huaqiao University, Xiamen 361021 China

*Corresponding author: e-mail: ben@micromaterials.co.uk

Keywords: Micro-impact, Fracture resistance, Elevated temperature, Titanium aluminium silicon nitride

Abstract

A high temperature micro-impact test has been developed to assess the fracture resistance of hard coatings under repetitive dynamic high strain rate loading at elevated temperatures. The test was used to study the temperature dependence of the resistance to micro-scale impact fatigue of TiAlSiN coatings on cemented carbide at 25-600 °C. Nanoindentation and micro-scratch tests were also performed over the same temperature range. The results of the micro-impact tests were dependent on the impact load, coating microstructure, coating and substrate mechanical properties, and their temperature dependence. At higher temperatures there was a change in failure mechanism from fracture-dominated to plasticity-dominated behaviour under the cyclic loading conditions. This was attributed to coating and substrate softening.

1. Introduction

Monolayered PVD (physical vapour deposition) ternary transition metal nitrides such as TiAlN and AlCrN have excellent wear resistance in metal cutting applications [1-11]. This is due to a combination of factors which act in synergy including improved oxidation resistance, thermal stability, age-hardening through spinodal decomposition and more protective tribofilm formation in comparison to binary nitrides such as TiN or CrN [12-14]. Despite this, hot microhardness and elevated temperature nanoindentation studies have shown that their hot hardness can decrease dramatically in comparison to room temperature measurements [15-19]. More advanced multilayer coatings and quaternary compositions are being developed with improved properties such as enhanced high temperature mechanical properties and wear resistance [19-36].

To obtain coating characterisation data under more controlled conditions than field trials small scale mechanical tests and instrumented accelerated laboratory wear tests are used. This enables rapid screening for promising compositions and optimisation of coating architectures. As they can easily and quickly be replicated they provide a statistical overview of coating performance. Nano- and micro-scale mechanical/tribological characterisation by the combination of indentation, scratch and impact tests has shown potential to improve our fundamental understanding of the link between coating properties and durability in cutting and streamline coating development.

To be a more reliable predictor of actual service performance it is important that the tests closely simulate the contact conditions so that the major wear mechanisms are replicated. Nano-impact testing with sharp cube corner diamond indenters has proved effective in simulating the highly loaded repetitive contact in interrupted turning and face and end milling applications with coating performance in the rapid lab-scale test showing strong correlation to their lifetime in the actual application [7,37,38]. Bouzakis and co-workers used the technique

to study influence of post-deposition coating treatment and the developed compressive stresses on coating brittleness and tool life [7]. They reported strong correlation between the results of nano-impact tests with a cube corner diamond probe and the cutting performance when milling hardened steel (AISI 4140) with micro-blasted Ti40Al60N coated cemented carbide tools. Focussed ion-beam cross-sectioning has been used to study deformation mechanisms in the nano-impact test. In nano-impact tests on multilayer titanium aluminium silicon nitride and monolayer TiN coatings on hardened tool steel with a cube corner probe at 10-150 mN a higher load was required for chipping in the multilayered TiAlSiN coating but there was no delamination on either coating [39].

By changing the applied load and probe geometry in the impact test, it is possible to alter the severity of the test and to move the positions of peak impact-induced stresses relative to the coating-substrate interface. Increasing the energy delivered per impact enables different indenter geometries to be used instead of the sharp cube corner. Tarrés and co-workers have noted that, by switching from sharp to blunter spherical indenters, there is an intrinsic suitability for examining damage evolution in bulk materials as a function of number of cycles [40]. By performing repetitive indentation tests at 50-4000 N with 0.5-2.5 mm radii cemented carbide indenters Ramírez and co-workers increased the test sensitivity to substrate properties at the expense of losing the influence of the coating on the yield behaviour [41].

Between the nano- and macro- impact a recently developed micro-impact test typically employs impact loads in the micro- range (~0.5-5 N) together with spheroconical diamond probes with end radii of ~10-50 μm. The maximum energy supplied per impact with the micro-impact technique is around 2 orders of magnitude greater than the maximum possible in the nano-impact technique. Nano- and micro-scale tests have been used in the study of the resistance to impact fatigue of Al-rich PVD nitride coatings on cemented carbide [42]. A

$Ti_{0.25}Al_{0.65}Cr_{0.1}N$ coating with high H^3/E^2 performed best in the nano- and micro- impact tests although it was not the hardest coating studied.

In applications such as turning, end milling and hot-forming high temperatures are generated in contact. The temperature dependence of mechanical properties will alter the wear rate and may change the predominant deformation mechanism. In these cases the results of room temperature tests are less relevant, Jinhal and co-workers reported that in hot hardness measurements over 600 °C the hardness of TiCN decreased more rapidly than TiAlN which was a factor in the superior tool life of TiAlN over TiCN in continuous turning of inconel and carbon steel [15]. The relative improvement of TiAlN over TiCN was more noticeable at higher cutting speeds where the contact temperature is greater. Although experimentally more challenging than at room temperature, nano- and micro- scale mechanical and tribological tests can be performed at elevated temperature. [11,37,38,42-44] High temperature micro-scratch tests have shown that the critical load at 500 °C can be larger than at room temperature [11,37]. Best and co-workers reported enhanced plastic deformation at 500 °C in high frequency impact testing of a 5 µm CrN coating with a 5 µm flat punch [44]. Fracture probability in nano-impact tests of $Ti_{0.5}Al_{0.5}N$ and $Al_{0.67}Ti_{0.33}N$ coatings decreased at 500°C compared to room temperature consistent with enhanced plasticity shown by nanoindentation [38].

In this current study we have performed nano- and micro-scale mechanical testing at elevated temperature on PVD TiAlSiN coatings. TiAlSiN coatings have better mechanical properties and thermal stability than TiAlN [21]. TiAlSiN has been reported to have 20 % longer tool life in milling hardened steel than TiAlN [25]. Addition of Si induces grain refinement and results in a dense microstructure more resistant to oxidation and contact fatigue [32]. These improved properties are believed to result from the formation of a nanocomposite TiAlSiN structure with cubic TiAlN embedded in an amorphous Si_3N_4 matrix. In high temperature tribological tests

on TiAlSiN wear rate was lower at 600 °C than 400 °C due to formation of protective tribofilms of Al_2O_3 and SiO_2 [27]. Tillmann and Dildrop reported that when sliding against WC-Co the coating wear rate was lower at 800 °C than 500 °C, particularly for higher Si-contents [22]. Fuentes [32] reported that when sliding against alumina the protective oxide-based tribo-film developed at 200-600 °C, with lower wear rates than at room temperature.

Multilayer nitride coatings have shown enhanced performance in tribological tests and machining applications [24, 29-31, 33-36]. In dry turning of Inconel 718 multilayer TiAlSiN showed improved performance in comparison to monolayer TiAlSiN [21]. In this current study nanoindentation, micro-scratch and micro-impact tests have been performed from 25 to 600 °C on monolayer TiAlSiN and TiAlN/TiSiN nano-multilayer coatings on cemented carbide. Although nano-impact tests have previously been performed at elevated temperatures up to 500 °C, [38] this study is the report of micro-scale impact testing performed at elevated temperature. The influence of the coating thickness to probe radius ratio and the temperature dependence of the mechanical properties of the coatings and the cemented carbide substrate on the behaviour in the micro-impact tests is discussed.

2. Experimental

2.1 Coating deposition

An Oerlikon Balzers INNOVENTA Mega coating deposition system with Ti and AlSi targets was used to deposit 2 µm monolayer PVD TiAlSiN on ISO P30 cemented carbide (75 wt % WC, 7% TiC, 8% TaC+NbC, 10 wt% Co). The deposition was carried out at 500 °C in a pure nitrogen atmosphere with substrate bias of -80 V and N_2 pressure of 2 Pa. Compositional analysis of the monolayer by energy dispersive x-ray analysis (EDX) = $Ti_{0.50}Al_{0.07}Si_{0.045}N_{0.38}$.

The same coating system was used with TiAl and TiSi targets and substrate rotation to deposit a 2 µm nano-multilayered PVD TiAlSiN composed of approximately 100 alternating TiAlN and TiSiN layers on ISO P30 cemented carbide. Compositional analysis of the nano-multilayer by EDX = $Ti_{0.48}Al_{0.19}Si_{0.022}N_{0.31}$. The coatings were polished prior to testing to remove droplets and reduce their surface roughness and improve the accuracy of the nanomechanical measurements.

2.2 Nanomechanical and micro-scratch characterisation at 25-600 °C

Nanoindentation and micro-scratch testing was performed with a NanoTest Vantage system (Micro Materials Ltd., Wrexham, UK). For the nanoindentation tests at room temperature a diamond Berkovich indenter was used to indent to a peak load of 30 mN at 3 mN/s. There was a 10 s hold at peak load before unloading at 3.75 mN/s. Thermal drift correction was from a 60 s hold at 90 % unloading. Hardness (H) and reduced elastic modulus (E_r) were determined from power-law fitting to the unloading curves. The elastic modulus (E) and Poisson ratio of the diamond indenter were 1141 GPa and 0.07 respectively. A coating Poisson's ratio of 0.25 was used to obtain the Young's modulus from the reduced modulus. A cubic Boron Nitride (cBN) Berkovich indenter was used for the high temperature nanoindentation tests at 400 ºC and 600 ºC which were performed in a purged argon environmental chamber. The elastic modulus and Poisson ratio of the cBN indenter were taken as 800 GPa and 0.12 respectively at room temperature. Between room temperature and 600 °C the Elastic modulus of the indenter decreases by less than 3 %. The temperature dependence of the elastic properties of the cBN indenter was taken into account when determining the E_s values at 400 and 600 °C. The samples were heated resistively and the temperature measured with a thermocouple placed immediately behind an AlN tile in the hot stage to which the sample was attached to with Resbond 908 high temperature adhesive. The sample and indenter were separately actively heated to ensure

isothermal contact and minimise thermal drift. The loading conditions for the high temperature tests were the same as in the room temperature tests.

A 25 μm end radius diamond conical indenter was used for the room temperature micro-scratch tests which were performed as 3-scan multi-pass topography-scratch-topography tests. The R_a surface roughness determined from the initial pass data was (0.022 ± 0.007) μm for the monolayer and (0.046 ± 0.016) μm for the nano-multilayer. In the ramped scratch pass, after a levelling distance of 100 μm the load was ramped to a peak load of 5 N at 55 mN/s. The scratch length was 2 mm. 3 repeat tests were performed on each sample. The contact load in the pre- and post- scratch topographic scans and the initial 100 μm of the ramped scratch was set at 0.3 mN. The same 25 μm end radius diamond conical indenter was used for the high temperature micro-scratch tests at 300 ºC and 600 ºC. Experimental conditions were the same as for the room temperature tests with a small modification to reduce the time in contact. To minimise the time in contact at elevated temperature the scratch length was reduced to 1.5 mm and the loading rate increased to 105 mN/s.

2.3 Micro-impact tests at 25-600 °C

A NanoTest Vantage was modified with a large electromagnet and indenter adapter arm to enable micro-impact tests to be performed. A schematic representation of the micro-impact configuration and a photograph showing its implementation in dual-loading head NanoTest Vantage system are shown in Figure 1 (a,b). The micro-impact tests on the TiAlSiN coatings were performed with a 90° spheroconical diamond indenter. The end radius of the indenter was determined as 17 μm by calibration with fused silica. Suitable experimental conditions to assess impact resistance of hard PVD coatings on WC-Co substrate were determined for this probe [42]. Repeat micro-impact tests were performed at 1, 1.2 and 1.5 N with an accelerating

distance of 40 μm. The test duration was 300 s with 1 impact every 4 s, resulting in 75 impacts in total. There were 3 repeats at 1 N, and at least 15 repeats at 1.2 and 1.5 N. The distance between repeat tests was 200 μm. Three additional tests at 1.5 N were performed with a larger accelerating distance of 60 μm.

Repetitive elevated temperature micro-impact tests at 1.5 N were performed at 300, 500 and 600 ºC. The test conditions were similar to those in the room temperature tests, although the time in contact was minimised by increasing impact frequency to 1 impact every 2 s and reducing the test duration to 150 s. The heating rate was set to 10 °C/min. In contrast to the elevated temperature nanoindentation tests, the micro-impact tests were performed without argon purging. To minimise oxidative degradation the probe was not actively heated. After the elevated temperature tests the indenter geometry was checked indirectly by re-testing samples that had not been exposed to high temperature under the same experimental conditions, and by indentation tests on fused silica. Since the impact probe was not actively heated some thermal drift was observed in the high temperature tests but its effect is lessened by the re-zeroing effect when the probe position is recorded out of contact as the position 40 μm above the surface stays approximately constant throughout the 150 or 300 s tests. Scanning electron microscopy (SEM) imaging of the micro-impact craters was performed using a FEI XL30 ESEM at 20 kV and a working distance of 6-8 mm with EDX analysis (Oxford instruments and Aztec software).

3. Results

3.1 Nanoindentation and micro-scratch tests

The variation in coating mechanical properties with increasing temperature is shown in Table 1. At room temperature the mechanical properties of both coatings are quite similar. Although the nano-multilayer was slightly harder this was accompanied by higher stiffness so the H/E

ratio of both coatings was almost the same. The nano-multilayer had higher resistance to plastic deformation, H^3/E^2. The coatings soften and become slightly lower in elastic modulus between 25 and 600 °C. Since the decrease in elastic modulus was less pronounced than the decrease in hardness the H/E ratio and, more significantly the H^3/E^2 parameter decrease with increasing temperature.

Coating failure in the depth-sensing micro-scratch tests was defined at the point at which there is a dramatic loss in the load-carrying capacity of the coating resulting in an abrupt increase in the on-load depth. Optical microscopy confirmed the onset of extensive cracking and chipping at this point. The critical load at which coating failure occurred in the micro-scratch test was found to vary only slightly with temperature (Table 2). The extent of scratch recovery up to failure was found to be strongly temperature dependent however, with significant scratch recovery at room temperature and minimal recovery in the higher temperature tests. In comparison with the brittle failure in room temperature scratch tests it was more difficult to assign a clear failure point from the scratch depth data in the high temperature tests due its more ductile nature.

3.2 Room temperature micro-impact

Illustrative plots of the impact depth vs. number of impacts are shown in Figure 1 (c,d). In all cases there is an abrupt increase in depth on initial impact due to the impact force being higher than the quasi-static load. During the first few impacts the impact depth increases then levels out. Thereafter the abrupt changes in probe depth are associated with fracture and material removal. The results for 40 μm accelerating distance are summarised in Table 3 (a,b). There was minimal difference between the coatings in their pre-impact static contact depth or in their resistance to a single impact. When there was no chipping of the coating the impact depth varied little with continuing impacts after the first few impacts (Fig. 1(c,d)). At 1 N the nano-

multilayer did not fracture in any of three repeat tests and the monolayer showed minor failure in only one of the three repeats (tests without fracture are shown in figure 1). With 40 μm accelerating distance clear load dependence in the coating fracture on repetitive impact was observed over 1-1.5 N. At 1.2 N the nanomultilayer fractured in a smaller number of tests than the monolayer. When the accelerating distance was increased to 60 μm both coatings failed rapidly at 1.5 N with more extreme damage thereafter in comparison to tests with 40 μm accelerating distance. Although the time-to-failure tended to be longer on the nanomultilayer the rate of damage thereafter was greater. This was particularly pronounced in the most severe tests (at 1.5 N, 60 μm accelerating distance).

SEM of the impact crater on multilayer at 1 N confirmed the absence of chipping at this load but faint concentric cracks were visible (fig. 2(a)). BS imaging of a crater on the monolayer at 1 N showed a partial ring crack (not shown). At higher load dramatic failure was observed (Figs 2 (b,c) and 3 (a,b)). BS imaging (e.g. fig. 2(c)) confirmed substrate exposure. EDX of the debris within the impact crater in figure 2(b,c) revealed that it was largely composed of the cemented carbide:- 1.7wt% Al; 5.8 wt% Ti; 10.1 wt% Co; 82.5 wt% W. The chipped region surrounding the impact crater was more extensive on the nanomultilayer.

3.3. High temperature micro-impact

Elevated temperature impact test results are summarised in Table 4 which records the variation in depth after the initial impact (i.e. depth after impact n – depth after initial impact). There was no observable change in indenter geometry after the elevated temperature tests. As the test temperature increased from 25-600 ºC the increase in impact depth on initial impact ($d(1)$-$d(0)$, depth after first impact minus the static depth) increased by ~300 nm on the monolayer and ~600 nm on the nanomultilayer. The increase in depth (d(failure)-$d(0)$) at which coating failure

occurred increased with the test temperature for the monolayer but was relatively unchanged on the nanomultilayer. The final impact depth (d(final)-d(0)) was higher when more brittle fracture occurred. Coating failure at elevated temperature was less pronounced on both coatings.

SEM images of typical craters after repetitive impact at 1.5 N at 300 °C, 500 °C and 600 °C are shown in Figure 4(a-c) for the monolayer and Figure 5(a-c) for the nanomultilayer. The differences in the extent of chipping outside the impact crater between the coatings observed at room temperature were also found at 300 °C (fig. 4(a), fig. 5 (a)). For both coatings there appears to be a change in mechanism between the sub-micron sized WC debris found at room temperature and a more ductile deformation mechanism at higher temperature with compacted substrate debris with some ring cracking observed within the compacted region. At 500 and 600 ºC the nanomultilayered coating shows significantly reduced coating fracture with only faint ring cracking observed at 600 ºC. After the testing at 600 ºC some discoloration of the nano-multilayer coating surface was observed optically but the appearance of the monolayer was unchanged.

Figure 6 (a) shows the depth change after initial impact from typical tests on the monolayer at 25-600 °C. The progression of coating damage is temperature dependent. The onset of failure requires less repetitive impacts at 300 and 500 °C than at room temperature but progresses more gradually at 500-600 °C than at lower temperature and the subsequent wear rate is lower. The depth change after initial impact in typical tests on the nanomultilayer at 25-600 °C is shown in Figure 6 (b). There is a marked temperature sensitivity with the nanomultilayered coating being more resistant to coating fracture at 500-600 °C.

4. Discussion

4.1. Room temperature impact behaviour

The higher H^3/E^2 and multilayered structure in the TiAlN/TiSiN nanomultilayer coating provide enhanced load carrying capability and resistance to crack initiation. Dissipative mechanisms are more limited in materials with high H^3/E^2 so that once cracks are initiated there is less resistance to crack propagation. This manifests itself in a larger chipped area and greater final impact depth for the nanomultilayer in the more severe impact tests. The switch in relative performance with test severity was also been reported by Zha and co-workers in high frequency (20 kHz) impact tests on these coatings with a 50 μm end radius diamond indenter [29]. Under low impact conditions the multilayer performed better but had worse cyclic impact resistance under more severe conditions. The micro-impact and high frequency impact tests show some correlation with cutting tests reported in [29]. In turning Ti6Al4V at 80 m/min the monolayer performed worse at low cutting force (feed rate = 0.1 mm/rev) but at higher cutting force (feed rate = 0.2 mm/rev) larger flank wear and spalling on the rake face was observed for the multilayer TiAlN/TiSiN. In micro-impact an micro-scratch tests of AlTiN and TiAlCrN coatings on WC-Co the coating with highest H^3/E^2 showed greater chipping outside the impact crater or scratch track [42].

In micro-scale impact tests the ratio between coating thickness h and indenter radius R is intermediate between nano-impact and macro-scale impact tests. As has been shown by finite element analysis, this influences the deformation mechanism [45]. In nano-impact with sharp cube corner probes the results are more dominated by the coating properties – chipping can be extensive but significant delamination is not observed on strongly adherent coatings [39]. In the micro-impact test this chipping is accompanied by substrate exposure at the edge of the impact crater and for WC-Co substrate, fatigue damage of the hard WC. In the micro-impact the results are strongly influenced by the coating and the substrate [42]. Figure 7 contrasts the behaviour of these TiAlSiN coatings on ISO P30 with a TiAlCrN monolayer on H10A

cemented carbide (previously tested in [42]). ISO with 10 wt. % Co has lower hardness and stiffness than the 6 wt. % Co H10A. The TiAlSiN coatings experience higher tensile and bending stresses due to reduced load support resulting in larger depth at failure and subsequently more rapid wear.

4.2 Elevated temperature behaviour

The performance of the TiAlSiN coatings in the micro-impact test was dependent on the impact load, coating microstructure, coating and substrate mechanical properties, and their temperature dependence. The high temperature nanoindentation data show the TiAlSiN coatings have excellent high temperature mechanical properties in comparison to other ternary and quarternary nitride coatings without Si incorporation. For the multilayer which has smaller % Si the hardness at 600 °C was 75 % of its room temperature value and for the monolayer with greater Si incorporation the hardness was 79 % of its room temperature value at 600 °C. The sharp probe (Berkovich) and small (~0.1) relative indentation depth (RID) in the high temperature nanoindentation tests mean the results are sensitive to coating properties with minimal substrate influence. ISO 14577 shows that there is some substrate influence at RID of ~0.1 but for coatings which are closely modulus matched to the cemented carbide substrate this should be almost negligible [46-48]. In the scratch and impact tests the larger applied loads and greater indenter radius used mean that the high temperature properties of the substrate also become important. As shown Milman and co-workers [49], the high Co fraction in the ISO P30 cemented carbide results in (i) lower room temperature hardness (ii) more rapid decrease in hardness with temperature than on cemented carbide grades such as H10A (a popular choice for substrate in previous elevated temperature nano- and micro-mechanical testing). This decrease in mechanical properties on P30 at elevated temperature is more important in the scratch and impact than in the indentation tests.

The TiAlSiN coatings display predominantly brittle behaviour at room temperature. In the high temperature micro-scratch tests there is reduced elastic recovery prior to failure due to the reduction in substrate hardness. The slight increase in critical load for the monolayer and invariant critical load on the multilayer appear to be a consequence of the reduced load support due to the decreased mechanical properties of the coating and substrate resulting in increased coating bending being offset by the reduced brittleness. As the critical load in the micro-scratch test is a function of probe radius any probe wear may have also a small effect. In previous micro-scratch tests of TiAlN, AlCrN and AlTiN coatings on H10A cemented carbide the critical load increased with temperature for AlCrN and AlTiN and decreased on TiAlN. Analytical modelling of the high temperature scratch data suggested that this was due to a changing stress distribution at temperature rather than an improvement in adhesion strength [11].

At higher temperatures there was a change in the dominant fatigue mechanism from fracture-dominated to more plasticity-dominated behaviour in the micro-impact tests. This transition to a milder wear mode occurs by 600 °C for the monolayer (fig. 6(a)) and by 500 °C for the nanomultilayer (fig. 6(b)). It has been suggested that grain refinement induced by Si incorporation in TiAlSiN can be responsible for reduction in thermal fatigue [32] but coating softening may also play a role. In elevated temperature nano-impact tests on $Ti_{0.5}Al_{0.5}N$ and $Al_{0.67}Ti_{0.33}N$ coatings on H10A the fracture probability decreased on both coatings at 500°C compared to that at room temperature which was consistent with enhanced coating plasticity at high temperature in nanoindentation tests [38]. In the micro-impact tests the improvement in behaviour at high temperature is a result of reduced coating *and substrate* brittleness. SEM imaging show a transition between fracture of WC grains resulting in sub-micron sized WC debris at lower temperature and a more ductile deformation mechanism at higher temperature. Goéz and co-workers have suggested that in designing for greater reliability cemented carbide

grades should be selected for optimal damage tolerance (i.e. deformation prevailing over fracture as the major damage mode) [50]. Analogously, increasing the temperature in the current study has a similar effect as moving to a tougher cemented carbide grade to change the main deformation mechanism by reducing brittle fracture.

The experimental conditions employed in this proof-of-concept pilot study could be refined in future optimisation of the technique. Unlike the high temperature nanoindentation tests with a cubic boron nitride indenter where active heating of indenter and sample was required to avoid heat flow and thermal drift, only the sample was actively heated in the micro-impact tests. This was a compromise to investigate whether an unheated diamond indenter could be used in these tests without environmental control without appreciable thermal drift or tip wear by reducing time in contact. With a heated probe oxidative damage of the diamond at 600 °C in air would have been unavoidable but with the approach taken there was no obvious wear of the indenter although it is unlikely probe degradation was completely eliminated. Planned development of the high temperature micro-impact test will investigate the use of different hard indenter materials, active probe heating and environmental control (e.g. by argon/forming gas purging or testing under vacuum).

5. Conclusions

The TiAlSiN coatings display predominantly brittle behaviour at room temperature. At lower load the TiAlN/TiSiN nanomultilayer displayed enhanced impact resistance but at higher load it showed more extensive chipping outside of the impact crater. The switch in relative performance of the coatings can be explained by the higher H^3/E^2 and multilayered structure in TiAlN/TiSiN which provide enhanced load carrying capability and resistance to crack initiation.

The high temperature nanoindentation data show the TiAlSiN coatings have excellent high temperature mechanical properties, retaining at least 75 % of their room temperature hardness at 600 °C. The feasibility of performing elevated temperature micro-impact tests with reduced contact time and without probe heating to minimise indenter wear in air has been demonstrated. At higher temperatures there was a change in the dominant fatigue mechanism from fracture-dominated to more plasticity-dominated behaviour in the micro-scratch and micro-impact tests. The improvement in behaviour at high temperature in the micro-impact test is due to reduced coating and substrate brittleness.

6. Acknowledgements

The novel micro-impact test technique was developed with the assistance of the Innovate UK Project No: 132369 – "Nano-to Micro-Impact Testing: An in-situ test for UK SEAC sector". Nick Pickford and Dr Stephen Goodes (both Micro Materials Ltd.) are acknowledged for modifying the NanoTest hardware and software respectively to develop the micro-impact capability. X. Zha (Huaqiao University) is thanked for his assistance with the coating deposition.

7. References

1. W. Kalss, A. Reiter, V. Derflinger, C. Gey, J.L. Endrino, Modern coatings in high performance cutting applications, Int. J. Refract. Met. Hard Mater. 24 (2006) 399-404.
2. G. Erkens, R. Cremer, T. Hamoudi, K.-D. Bouzakis, I. Mirisidis, S. Hadjiyiannis, G. Skordaris, A. Asimakopoulos, S. Kombogiannis, J. Anastopoulos, K. Efstathiou, Properties and performance of high aluminium containing (Ti,Al)N based supernitride coatings in innovative cutting applications, Surf. Coat. Technol. 177-178 (2004) 727-734.

3. J.L. Endrino, G.S. Fox-Rabinovich, C. Gey, Hard AlTiN, AlCrN PVD coatings for machining of austenitic stainless steel, Surf. Coat. Technol. 200 (2006) 6840-6845.
4. K.-D. Bouzakis, S. Hadjiyiannis, G. Skordaris, I. Mirisidis, N. Michailidis, K. Efstathiou, E. Pavlidou, G. Erkens, R. Cremer, S. Rambadi, I. Wirth, The effect of coating thickness, mechanical strength and hardness properties on the milling performance of PVD coated cemented carbide inserts, Surf. Coat. Technol. 177-178 (2004) 657-664.
5. A. Inspektor and P.A. Salvador, Architecture of PVD coatings for metalcutting applications: a review, Surf. Coat. Technol. 257 (2014) 138-153.
6. B.D. Beake, L. Ning, C. Gey, S.C. Veldhuis, A. Komarov, A. Weaver, M. Khanna, G.S. Fox-Rabinovich, Wear performance of different PVD coatings during wet end milling of H13 tool steel, Surf. Coat. Technol. 279 (2015) 118-125.
7. K.-D. Bouzakis, F.Flocke, G. Skordaris, E. Bouzakis, S. Geradis, G. Katirtzoglou and S. Makrimallakis, Influence of dry micro-blasting grain quality on wear behaviour of TiAlN coated tools, Wear 271 (2011) 783-791.
8. K.-D. Bouzakis, N. Michailidis, G. Skordaris, E. Bouzakis, D. Biermann, R. M'Saoubi, Cutting with coated tools: coating technologies, characterization methods and performance optimisation, CRIP Ann. Manuf. Technol. 61 (2012) 703-723.
9. A. Hörling, L. Hultman, M. Odén, J. Sjölén, L. Karlsson, Mechanical properties and machining performance of $Ti_{1-x}Al_xN$-coated cutting tools, Surf. Coat. Technol. 191 (2005) 384-392.
10. N. Michailidis, Variations in the cutting performance of PVD-coated tools in milling Ti6Al4V, explained through temperature-dependent coating properties, Surf. Coat. Technol. 304 (2016) 325-329.

11. B.D. Beake, J.L. Endrino, C. Kimpton, G.S. Fox-Rabinovich, S.C. Veldhuis, Elevated temperature repetitive micro-scratch testing of AlCrN, TiAlN and AlTiN PVD coatings, Int. J. Refract. Met. Hard Mater. 69 (2017) 215-226.
12. L. Hultman, C. Mitterer, Thermal stability of advanced nanostructured wear-resistant coatings, chapter 11 in: Nanostructured coatings, A. Cavaleiro and J.Th.M. De Hosson, eds., Springer, New York, 2006, pp464-510.
13. L. Chen, J. Paulitsch, Y. Du, P.H. Mayrhofer, Thermal stability and oxidation resistance of Ti-Al-N coatings, Surf. Coat. Technol. 206 (2012) 2954-2960.
14. G.S. Fox-Rabinovich, J.L. Endrino, B.D. Beake, M.H. Aguirre, S.C. Veldhuis, D.T. Quinto, C.E. Bauer, A.I. Kovalev, A. Gray, Effect of annealing below 900°C on structure, properties and tool life of an AlTiN coating under various cutting conditions, Surf. Coat. Technol. 202 (2008) 2985-2992.
15. P.C. Jinhal, A.T. Santhanam, U. Schleinkofer, A.F. Shuster, Performance of PVD TiN, TiCN and TiAlN coated cemented carbide tools in machining, Int. J. Refract. Met. Hard Mater. 17 (1999) 163-170.
16. D.T. Quinto, G.J. Wolfe, P.C. Jinhal, High temperature microhardness of hard coatings produced by physical vapour deposition, Thin Solid Films 153 (1987) 19-36.
17. M.H. Staia, M. D'Alessandria, D.T. Quinto, F. Roudet, M. Marsal Astort, High-temperature tribological characterisation of commercial TiAlN coatings, J. Phys.: Condens. Matter. 18 (2006) S1727-S1736.
18. B.D. Beake, G.S. Fox-Rabinovich, S.C. Veldhuis, S.R. Goodes, Coating optimisation for high-speed machining with advanced nanomechanical test methods, Surf. Coat. Technol., 203 (2009) 1919-1925.

19. B.D. Beake, G.S. Fox-Rabinovich, Progress in high temperature nanomechanical testing of coatings for optimising their performance in high speed machining, Surf. Coat. Technol. 255 (2014) 1021115.
20. G.S. Fox-Rabinovich, K. Yamamoto, S.C. Veldhuis, A.I. Kovalev and G.K. Dosbaeva, Tribological adaptability of TiAlCrN PVD coatings under high performance dry machining conditions, Surf. Coat. Technol. 200 (2005) 1804-1813.
21. G. Li, J. Sun, Y. Xu, J. Gu, L. Wang, K. Huang, K. Liu, L. Li, Microstructure, mechanical properties, and cutting performance of TiAlSiN multilayer coatings prepared by HiPIMS, Surf. Coat. Technol. 353 (2018) 274-281.
22. W. Tillmann, M. Dildrop, Influence of Si content on mechanical properties and tribological performance of TiAlSiN coatings at elevated temperatures, Surf. Coat. Technol. 321 (2017) 448-454.
23. Q. Ma, L. Li, Y. Xu, X. Ma, H. Liu, Effect of Ti content on the microstructure and mechanical properties of TiAlSiN nanocomposite coatings, Int. J. Refract. Met. Hard Mater. 59 (2016) 114-120.
24. Q. Zhang, Y. Xu, T. Zhang, Z. Wu, Q. Wang, Tribological properties, oxidation resistance and turning performance of AlTiN/AlCrSiN multilayer coatings by arc ion plating, Surf. Coat. Technol. 356 (2018) 1-10.
25. D. Yu, C. Wang, X. Cheng, F. Zhang, Microstructure and properties of TiAlSiN coatings prepared by hybrid PVD technology, Thin Solid Films 517 (2009) 4950-4955.
26. Q. Ma, L. Li, Y. Xu, J. Gu, L. Wang, Y. Xu, Effect of bias voltage on TiAlSiN nanocomposite coatings deposited by HiPIMS, Appl. Surf. Sci. 392 (2017) 826-833.
27. N. He, H. Li, L. Ji, X. Liu, H. Zhou, J. Chen, High temperature tribological properties of TiAlSiN coatings produced by hybrid PVD technology, Tribol. Int. 98 (2016) 133-143.

28. F. Cao, P. Munroe, Z. Zhou, Z. Xie, Mechanically robust TiAlSiN coatings prepared by pulsed-DC magnetron sputtering system: scratch response and tribological performance, Thin Solid Films 645 (2018) 222-230.
29. X. Zha, F. Jiang, X. Xu, Investigating the high frequency fatigue failure mechanisms of mono and multilayer PVD coatings by the cyclic impact tests, Surf. Coat. Technol. 344 (2018) 689-701.
30. J.J. Roa, E. Jiménez-Pique, R. Martínez, G. Ramírez, J.J. Tarragó, R. Rodríquez, L. Llanes, Contact damage and fracture micromechanisms of multi-layered TiN/CrN coatings at micro- and nano-length scales, Thin Solid Films 571 (2014) 308-315.
31. Y.-Y. Chang, C.-J. Wu, Mechanical properties and impact resistance of multi-layered TiAlN/ZrN coatings, Surf. Coat. Technol. 231 (2013) 62-66.
32. G.G. Fuentes, E. Almandoz, R.J. Rodríquez, H. Dong, Y. Qin, S. Mato, F.J. Pérez-Trujillo, Vapour deposition technologies for the fabrication of hot-forming tools, Manufacturing Rev. 1 (2014) 20.
33. Y.X. Ou, J. Lin, H.L. Che, W.D. Sproul, J.J. Moore, M.K. Lei, Mechanical and tribological properties of CrN/TiN multilayer coatings deposited by pulsed dc magnetron sputtering, Surf. Coat. Technol. 276 (2015) 152-159.
34. C. Mendibide, P. Steyer, J. Fontaine, P. Goudeau, Improvement of the tribological behaviour of PVD nanostratified TiN/CrN coatings – an explanation, Surf. Coat. Technol. 201 (2006) 4119-4124.
35. C. Mendibide, J. Fontaine, P. Steyer, C. Esnoul, Dry sliding wear model of nanometer scale multi-layered TiN/CrN PVD hard coatings, Tribol. Lett. 17 (2004) 779-789.
36. A.A. Vereschaka, S.N. Grigoriev, Study of cracking mechanisms in multi-layered composite nano-structured coatings, Wear 378-379 (2017) 43-57.

37. G.S. Fox-Rabinovich, B.D. Beake, S.C. Veldhuis, J.L. Endrino, R. Parkinson, L.S. Shuster, M.S. Migranov, Impact of mechanical properties measured at room and elevated temperatures on wear resistance of cutting tools with TiAlN and AlCrN coatings, Surf. Coat. Technol. 200 (2006) 5738-5742.
38. B.D. Beake, J.F. Smith, A. Gray, G.S. Fox-Rabinovich, S.C. Veldhuis, J.L. Endrino, Investigating the correlation between nano-impact fracture resistance and hardness/modulus ratio from nanoindentation at 25-500ºC and the fracture resistance and lifetime of cutting tools with Ti1-xAlxN (x = 0.5 and 0.67) PVD coatings in milling operations, Surf. Coat. Technol. 201 (2007) 4585-4593.
39. J. Chen, R. Ji, R.H.U. Khan, X. Li, B.D. Beake and H. Dong, Effects of mechanical properties and layer structure on the cyclic loading of TiN-based coatings Surf. Coat. Technol. 206 (2011) 522-529.
40. E. Tarrés, G. Ramírez, Y. Gaillard, E. Jiménez-Piqué and L. Llanes, Contact fatigue behaviour of PVD-coated hardmetals, Int. J. Refract. Met. Hard Mater. 27 (2009) 323-341.
41. G. Ramírez, A. Mestra, B. Casas, I. Valls, R. Martínez, R. Bueno, A. Góez, A. Mateo, L. Llanes, Influence of substrate microstructure on the contact fatigue strength of coated cold-work tool steels, Surf. Coat. Technol. 206 (2012) 3069-3081.
42. B.D. Beake, L. Isern, J.L. Endrino, G.S. Fox-Rabinovich, Micro-impact testing of AlTiN and TiAlCrN coatings, Wear 418-419 (2019) 102-110.
43. A Review on Micro- and Nanoscratching/Tribology at High Temperatures: Instrumentation and Experimentation, S.Z. Chavoshi and S. Xu, JMEPEG 27 (2018) 3844-3858.
44. High temperature impact testing of a thin hard coating using a novel high-frequency in situ micromechanical device, J.P. Best, G. Guillonneau, S. Grop, A.A. Taylor, D. Frey,

Q. Longchamp, T. Schär, M. Morstein, J.-M. Breguet, J. Michler, Surf. Coat. Technol. 333 (2018) 178-186.

45. J. Michler, E. Blank, Analysis of coating fracture and substrate plasticity induced by spherical indentors: diamond and diamond-like carbon layers on steel substrates, Thin Solid Films 381 (2001) 119-134.
46. ISO 14577: Metallic Materials—Instrumented Indentation Test for Hardness and Materials Parameters, Parts 1-4 (revised 2015).
47. Determination of the hardness and modulus of thin films and coatings (INDICOAT), N.M. Jennett, A.S. Maxwell, K. Lawrence, L.N. McCartney, R. Hunt, J. Koskinen, J. Meneve, W, Wegener, T, Muukkonen. F. Rossi, N. Gibson, Zhihui Xu. A.J. Bushby, S. Brookes, A. Cavaleiro. K. Herrmann, B. Bellaton, R. Consiglio, F. Augereau, 0. Kolosov, D. Schneider, T. Chudoba, NPL Report MATC(A) Mat 24, 2001, ISSN 1473-2734. EU-funded project SMT4-CT98-2249.
48. N.M. Jennett, A.J. Bushby, Adaptive protocol for robust estimates of coatings properties by nanoindentation, Mater. Res. Soc. Symp. Proc. 695 (2002) 73-78.
49. Y.V. Milman, S. Luyckx, I.T. Northrop, Influence of temperature, grain size and cobalt content on the hardness of WC-Co alloys, Int. J. Refract. Met. Hard Mater. 17 (1999) 39-44.
50. A. Góez, D. Coureaux, A. Ingebrand, B. Reig, E. Tarrés, A. Mateo, E. Jiménez-Piqué, L. Llanes, Contact damage and residual strength in hardmetals, Int. J. Refract. Metal. Hard Mater. 30 (2012) 121-127.

Tables

Table 1 Elevated temperature nanoindentation data

	Temperature/ºC	H (GPa)	E (GPa)	H/E	H^3/E^2 (GPa)
monolayer	25	33.2 ± 2.8	521 ± 8	0.064	0.135
	400	29.4 ± 2.5	537 ± 8	0.055	0.088
	600	26.3 ± 2.0	514 ± 31	0.051	0.069
nano-multilayer	25	36.8 ± 3.1	564 ± 6	0.065	0.157
	400	32.2 ± 1.5	560 ± 15	0.058	0.106
	600	27.6 ± 0.8	539 ± 19	0.051	0.072

Table 2 Elevated temperature micro-scratch data

	Temperature/ºC	L_c (N)
monolayer	25	2.1 ± 0.2
	300	2.3 ± 0.2
	600	2.4 ± 0.3
nano-multilayer	25	2.5 ± 0.1
	300	2.6 ± 0.5
	600	2.5 ± 0.1

Table 3 (a) Room temperature micro-impact data on Monolayer TiAlSiN

	Applied Load and accelerating distance			
	1.5 N / 40 μm	1.5 N / 40 μm	1.5 N / 40 μm	1.5 N / 40 μm
Pre-impact depth (μm)	0.4 ± 0.0	0.7 ± 0.1	0.9 ± 0.1	0.8 ± 0.1
Depth on first impact (μm)	1.9 ± 0.1	2.2 ± 0.1	2.6 ± 0.1	3.0 ± 0.2
Failure probability	1/3	16/16	25/25	3/3
Time to failure (s)	275 ± 42	81 ± 44	70 ± 54	16 ± 8
Depth at failure (μm)	2.6	2.8 ± 0.1	3.3 ± 0.2	3.4 ± 0.2
Final depth (μm)	2.6 ± 0.4	4.9 ± 0.6	5.8 ± 0.7	6.8 ± 1.4

Table 3 (b) Room temperature micro-impact data on TiAlN/TiSiN multilayer

	Applied Load and accelerating distance			
	1.5 N / 40 μm	1.5 N / 40 μm	1.5 N / 40 μm	1.5 N / 40 μm
Pre-impact depth (μm)	0.5 ± 0.00	0.7 ± 0.0	0.9 ± 0.1	0.7 ± 0.0
Depth on first impact (μm)	1.7 ± 0.0	2.2 ± 0.1	2.6 ± 0.2	2.8 ± 0.1
Failure probability	3/3	7/15	22/23	3/3
Time to failure (s)	>300	212 ± 102	95 ± 73	40 ± 12
Depth at failure (μm)	-	2.8 ± 0.2	3.4 ± 0.3	3.7 ± 0.2
Final depth (μm)	2.2 ± 0.0	4.0 ± 1.4	6.0 ± 1.1	8.1 ± 0.6

Mean time to failure calculated assigning a value of 300 s for tests without failure.

Table 4 Temperature dependence of micro-impact behaviour at 1.5 N

		25 ºC	300 ºC	500 ºC	600 ºC
TiAlSiN	*d*(1)-*d*(0) (µm)	1.8 ± 0.1	2.2 ± 0.1	2.4 ± 0.0	2.4 ± 0.1
	d(fail)-*d*(0) (µm)	2.5 ± 0.1	2.9 ± 0.2	3.2 ± 0.1	3.2 ± 0.1
	d(final)-*d*(0) (µm)	5.3 ± 0.6	4.4 ± 0.1	4.7 ± 0.1	4.3 ± 0.4
TiAlN/TiSiN	*d*(1)-*d*(0) (µm)	1.8 ± 0.2	1.8 ± 0.2	2.2 ± 0.1	2.1 ± 0.1
	d(fail)-*d*(0) (µm)	2.6 ± 0.2	2.6 ± 0.1	2.7*	§
	d(final)-*d*(0) (µm)	4.8 ± 1.1	4.2 ± 0.5	3.1 ± 0.2	2.7 ± 0.1

Accelerating distance = 40 µm. *d*(1) = depth after initial impact. *d*(0) = static indentation depth (pre-impact, predominantly elastic). * Brittle failure only in 1 test at 500 ºC. § No failures at 600 ºC.

Figure captions

1. (a) Schematic representation of the micro-impact configuration. (b) High-temperature micro-impact implementation in dual-loading head NanoTest Vantage system. Illustrative impact depth vs. number of impacts data at room temperature for (c) monolayer TiAlSiN (d) TiAlN/TiSiN. The accelerating distance was 40 μm unless otherwise stated.

2. SEM of crater on multilayer after repetitive impact at 25 °C at (a) 1 N, SE image (b), 1.5 N SE image (c) 1.5 N BS image.

3. SEM of crater on monolayer after repetitive impact at 25 °C at (a) 1.5 N SE image (b) 1.5 N BS image.

4. SEM of craters on monolayer after repetitive impact at 1.5 N at (a) 300 °C, (b) 500 °C, (c) 600 °C.

5. SEM of craters on multilayer after repetitive impact at 1.5 N at (a) 300 °C, (b) 500 °C, (c) 600 °C.

6. Depth change after initial impact at 25-600 °C on (a) monolayer and (b) multilayer.

7. Comparative impact depth data at 1.5 N.

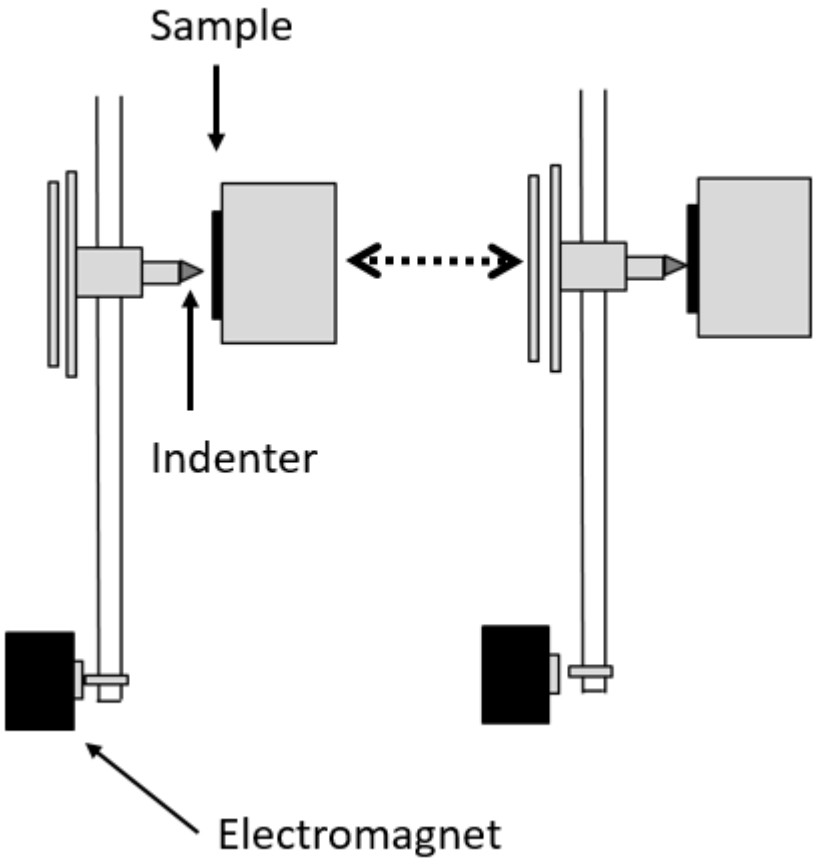
Sample
Indenter
Electromagnet

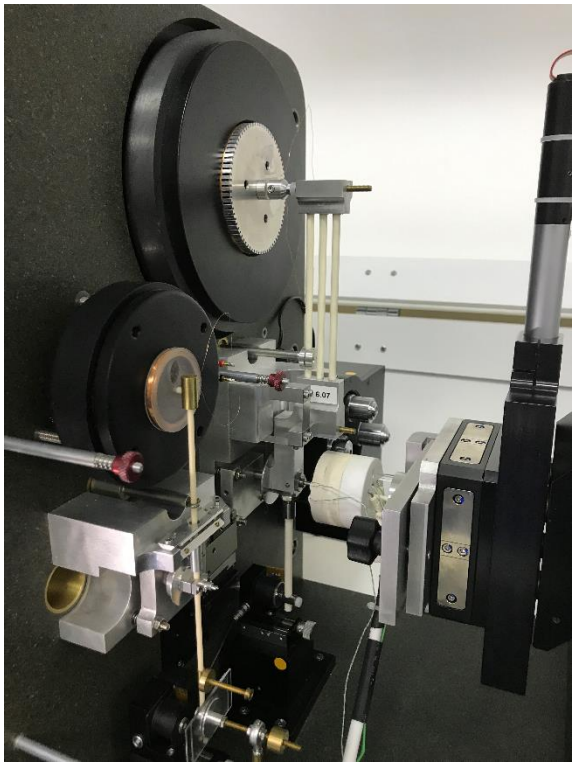

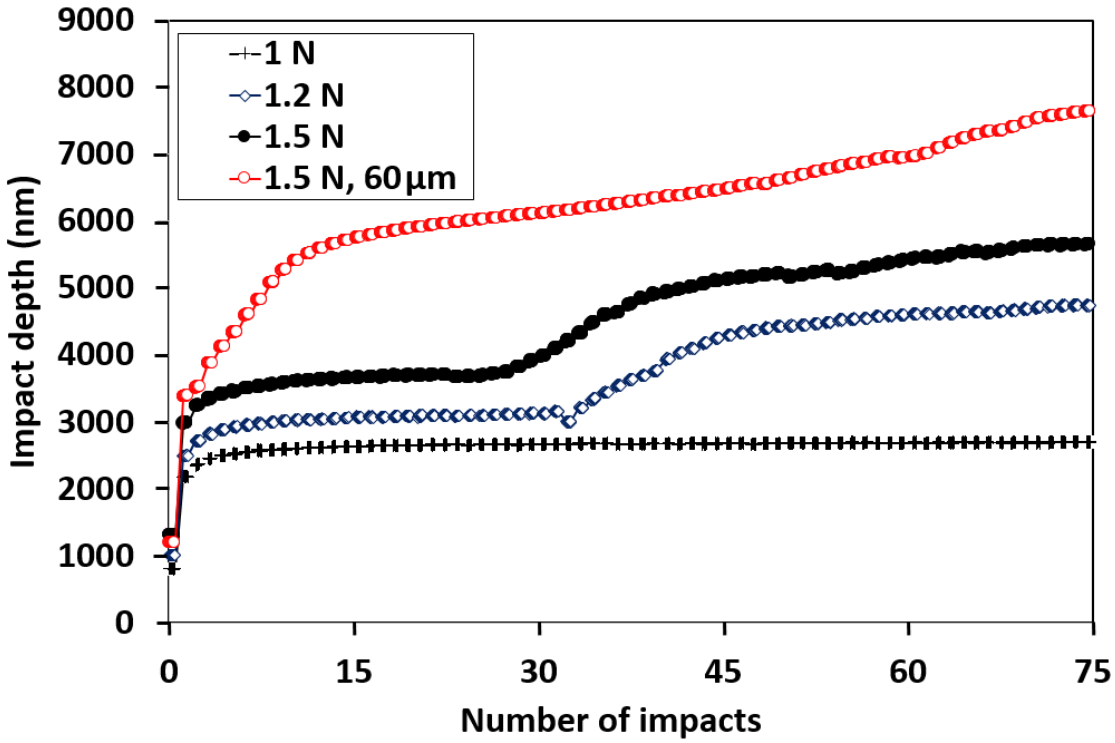
1 N
1.2 N
1.5 N
1.5 N, 60 µm
Impact depth (nm)
Number of impacts
0
1000
2000
3000
4000
5000
6000
7000
8000
9000
0
15
30
45
60
75

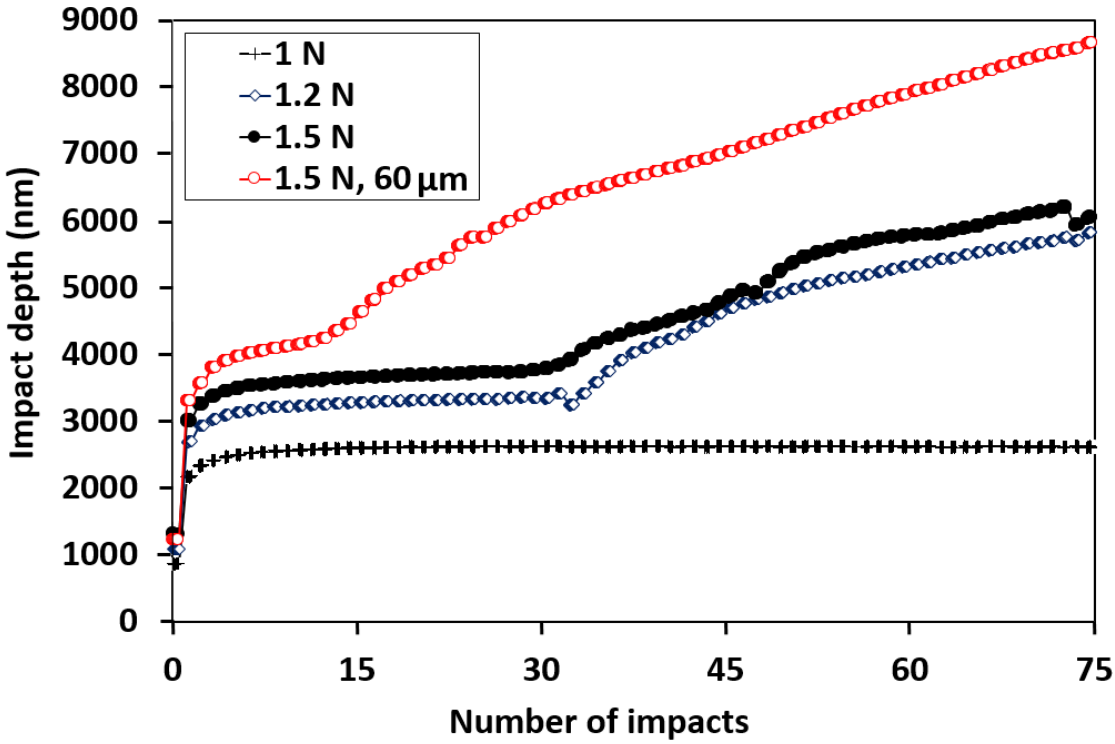
1 N
1.2 N
1.5 N
1.5 N, 60 µm
Impact depth (nm)
Number of impacts
0
1000
2000
3000
4000
5000
6000
7000
8000
9000
0
15
30
45
60
75

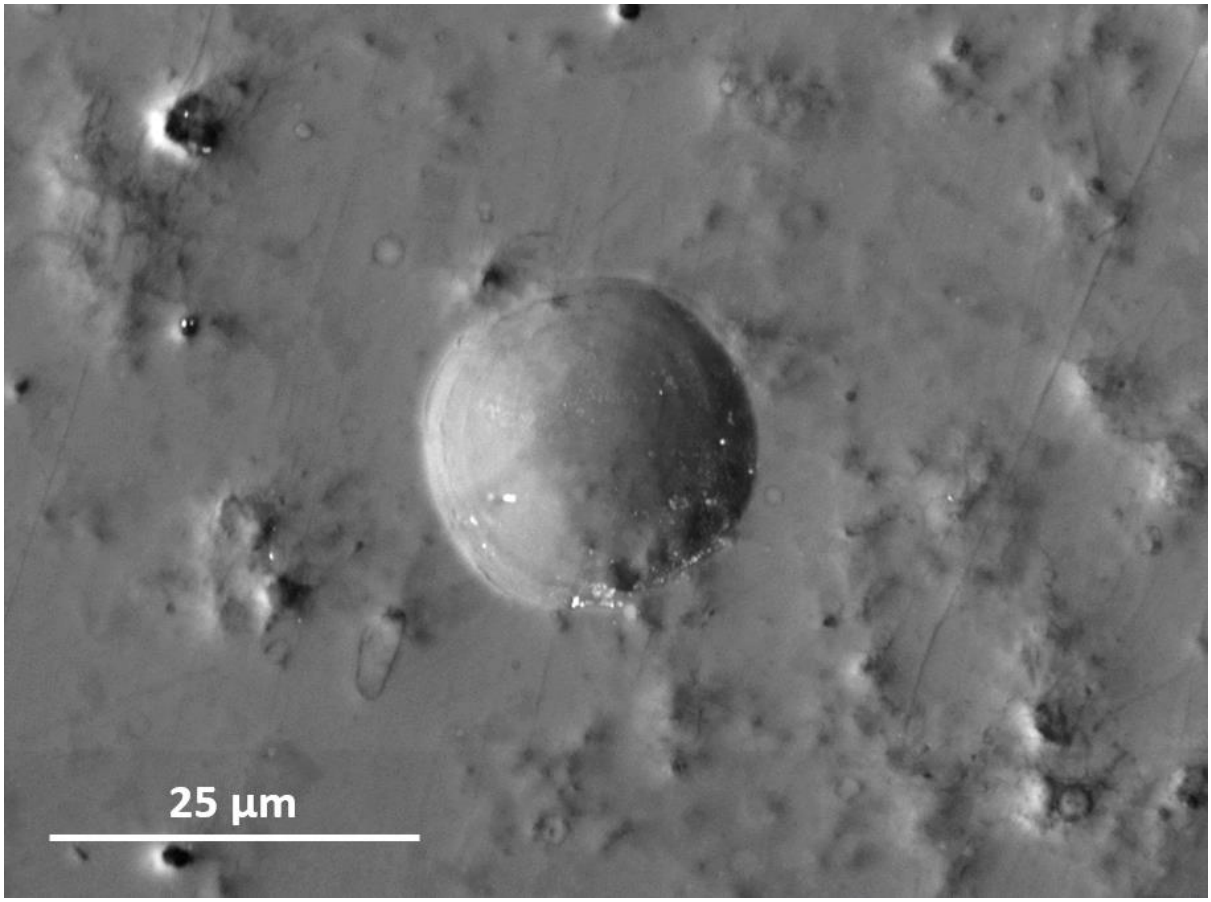
25 µm

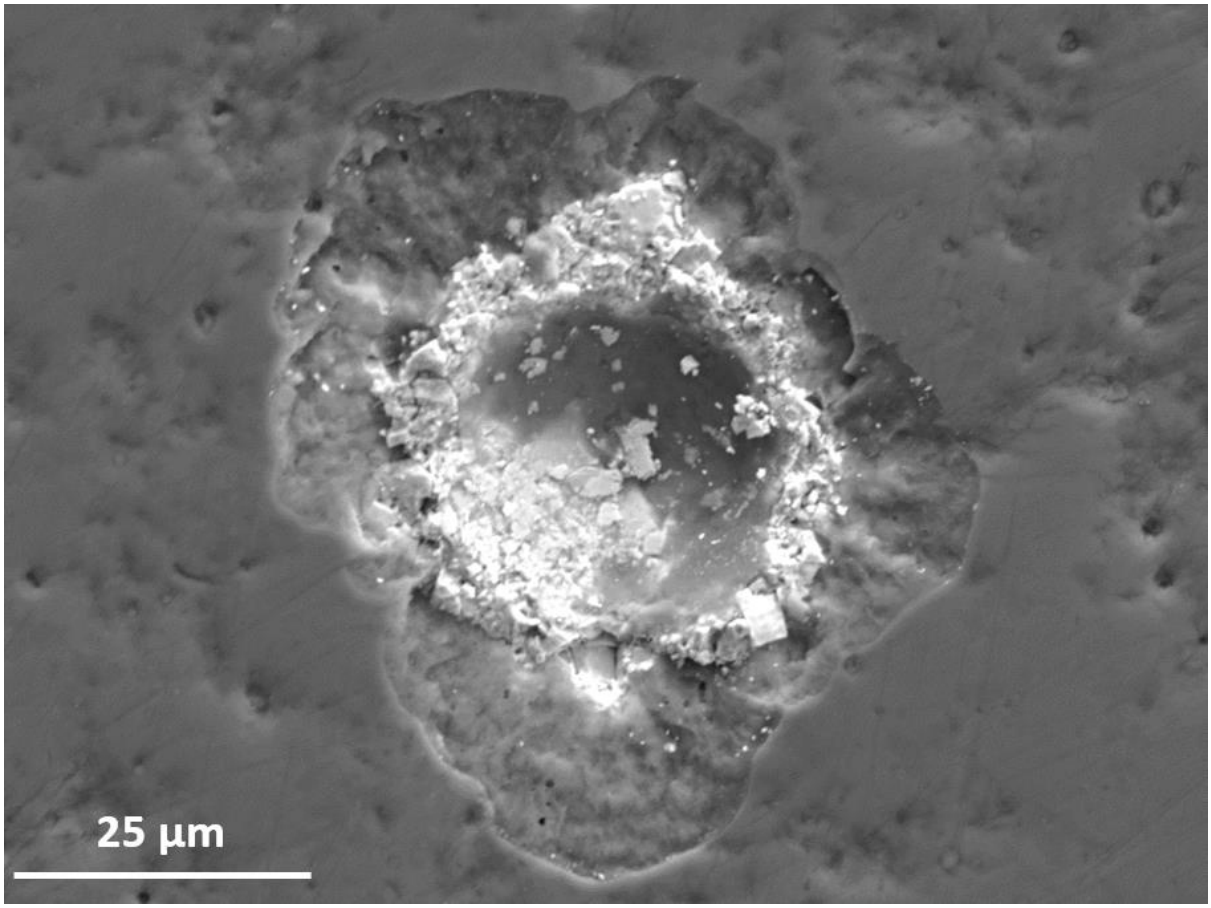
25 µm

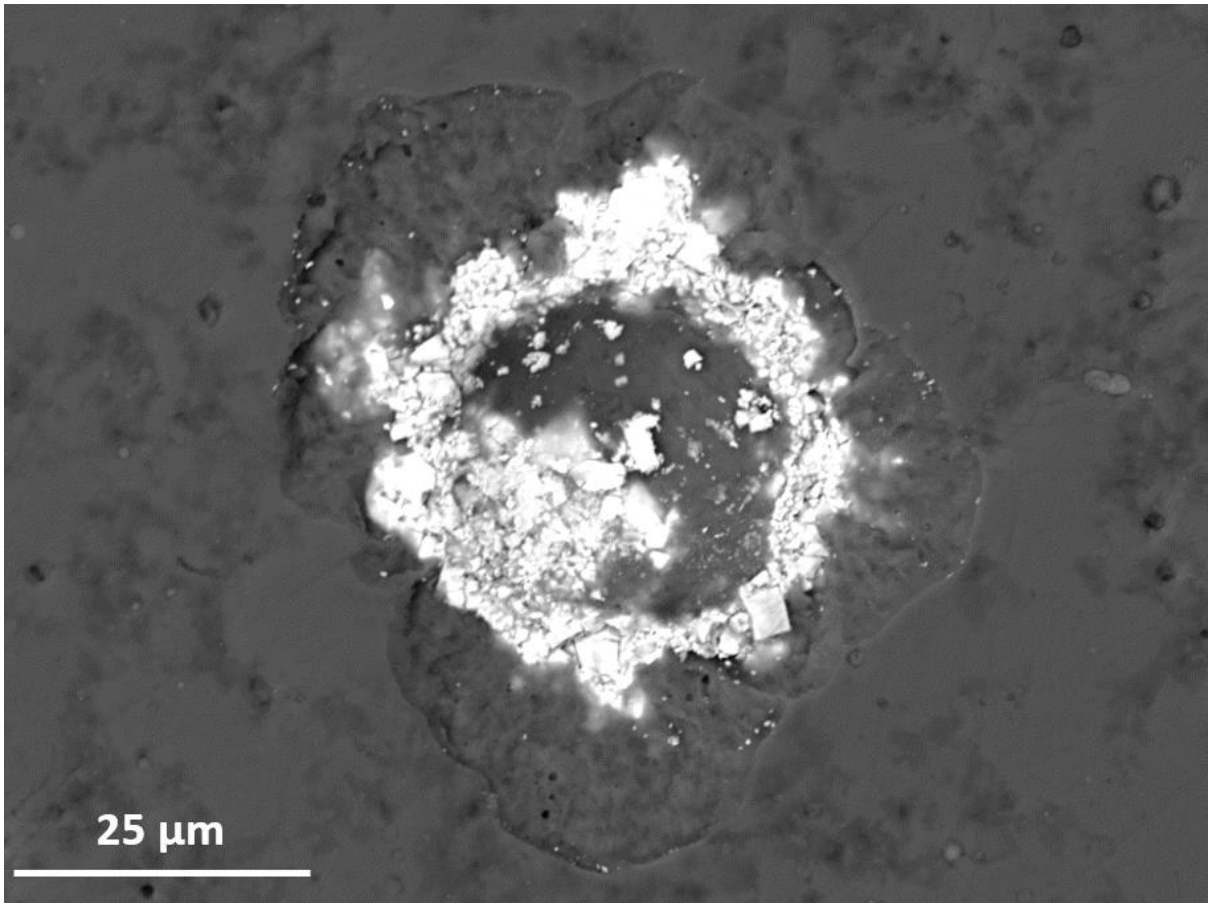
25 µm

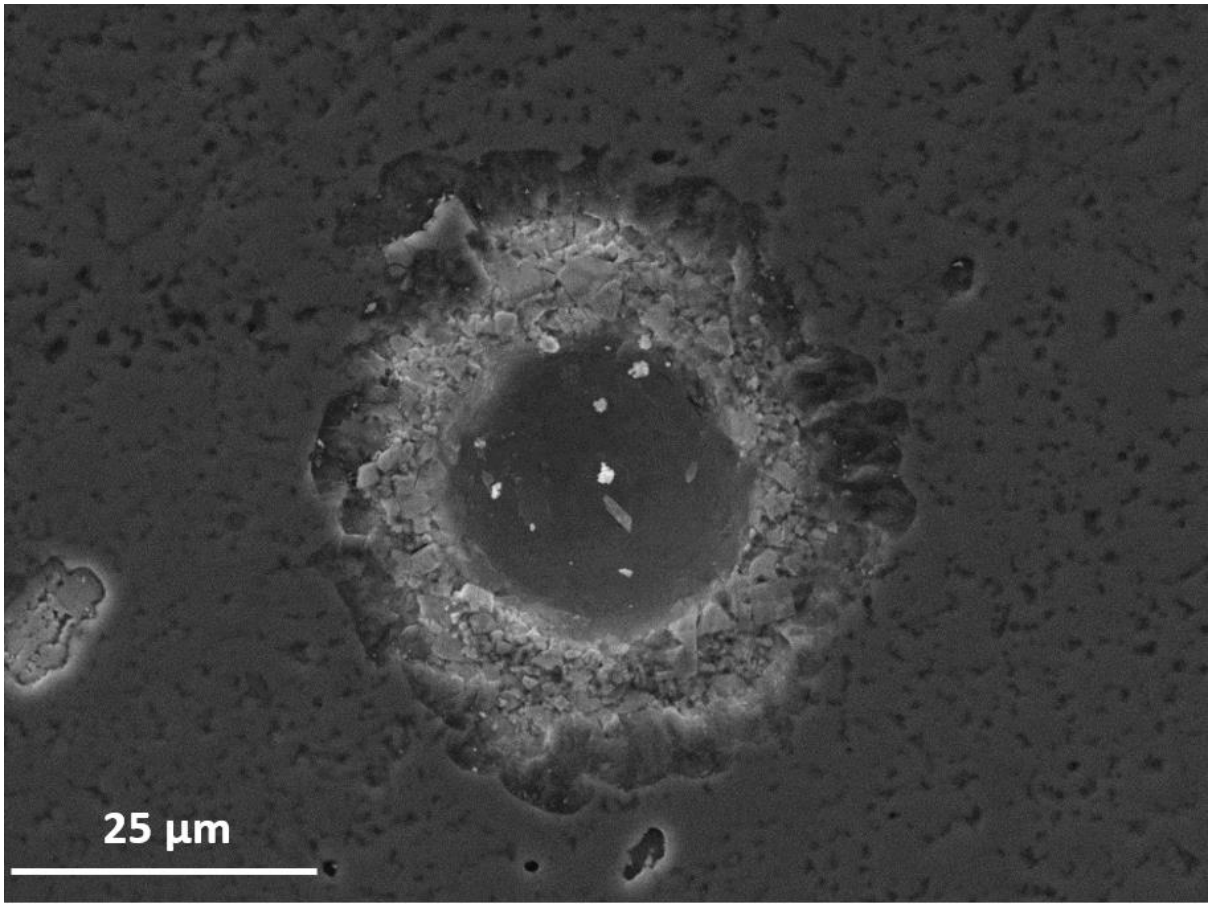
25 µm

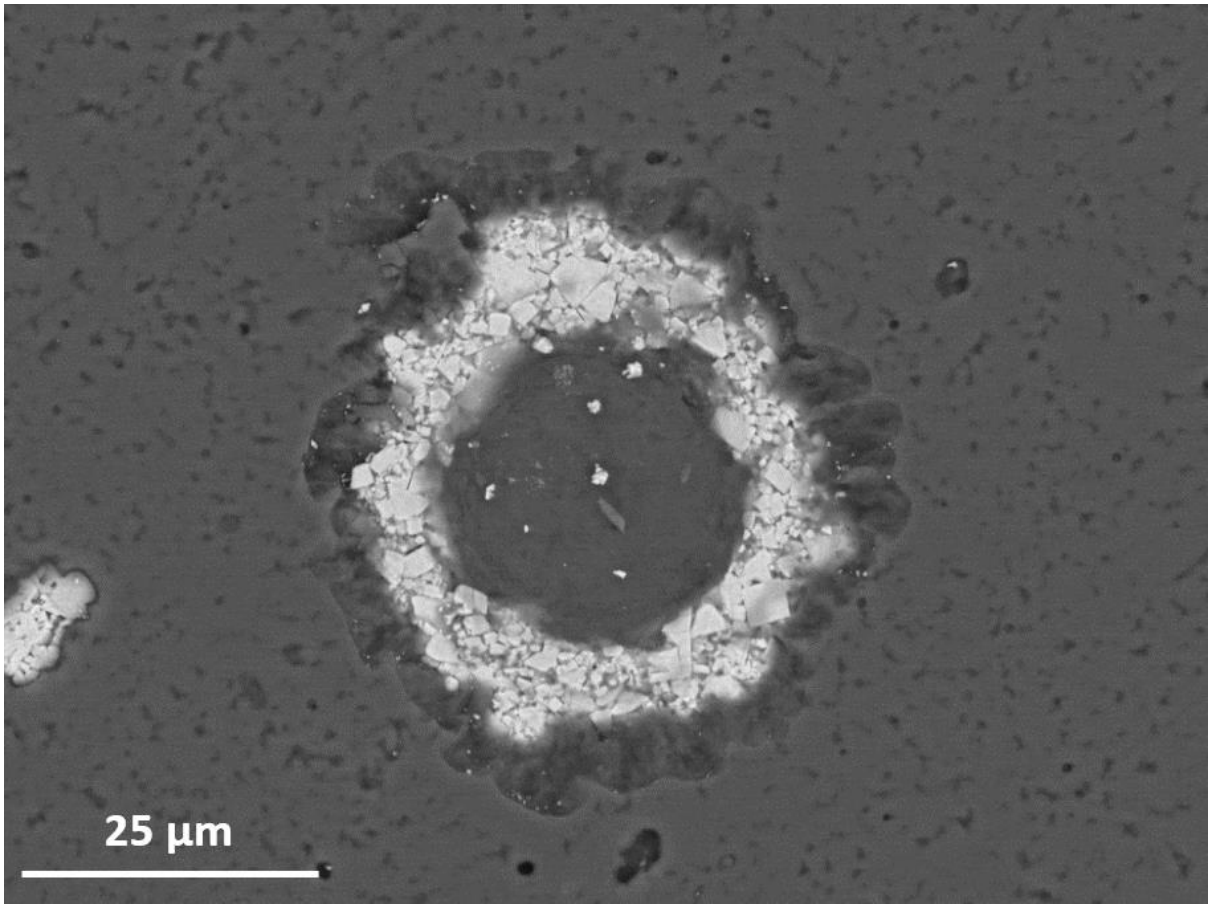
25 µm

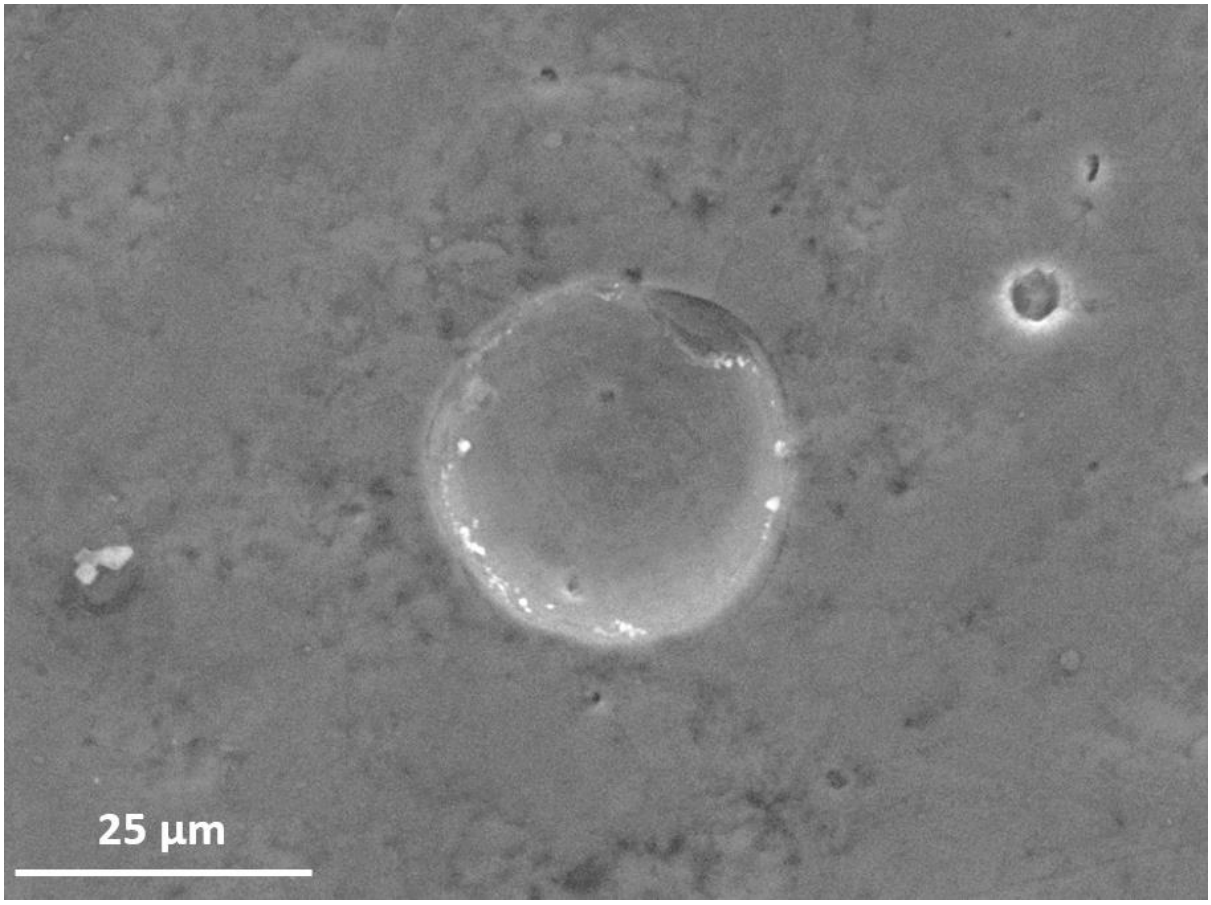
25 µm

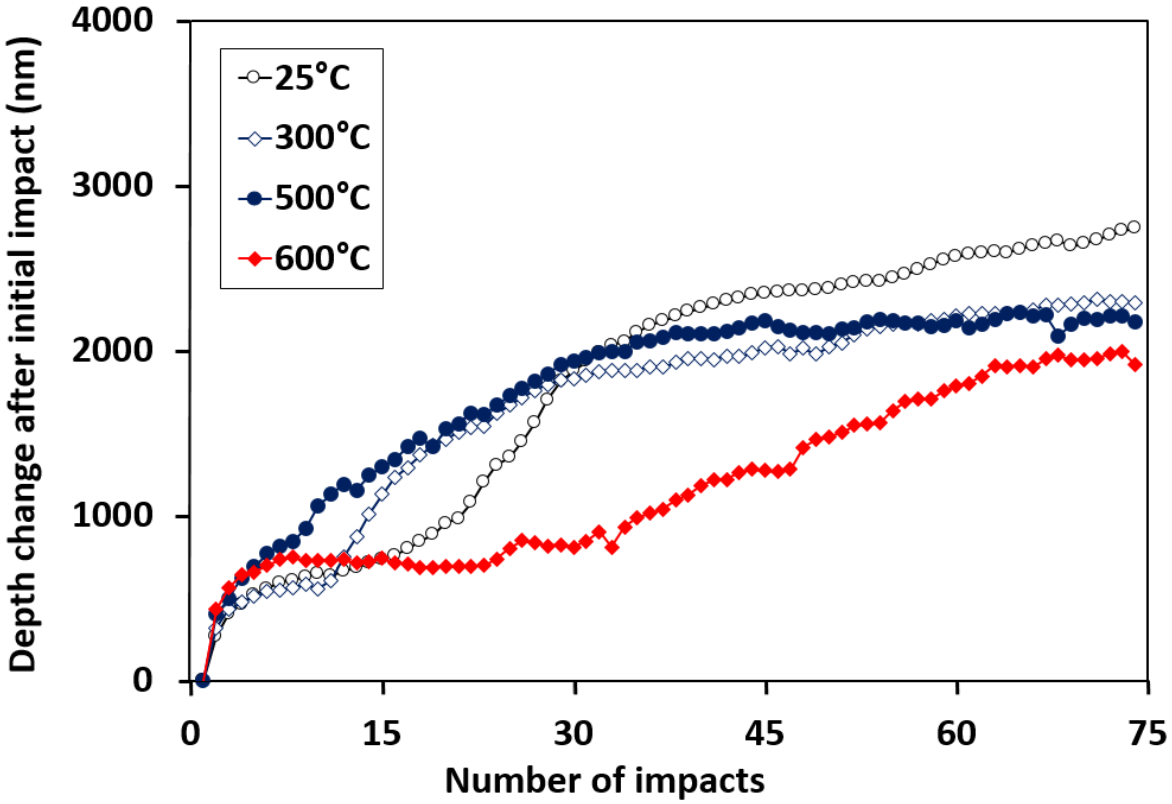
Depth change after initial impact (nm)
4000
3000
2000
1000
0
25°C
300°C
500°C
600°C
0
15
30
45
60
75
Number of impacts

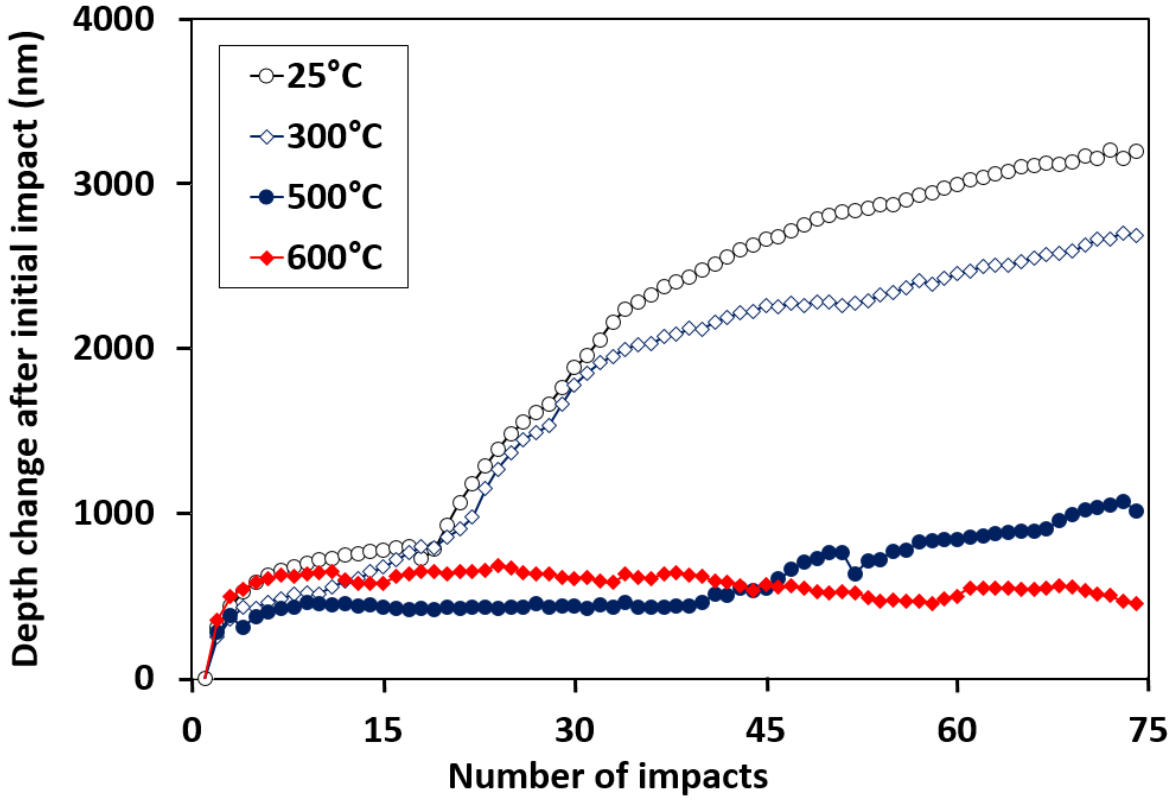
Depth change after initial impact (nm)
4000
3000
2000
1000
0
25°C
300°C
500°C
600°C
0
15
30
45
60
75
Number of impacts

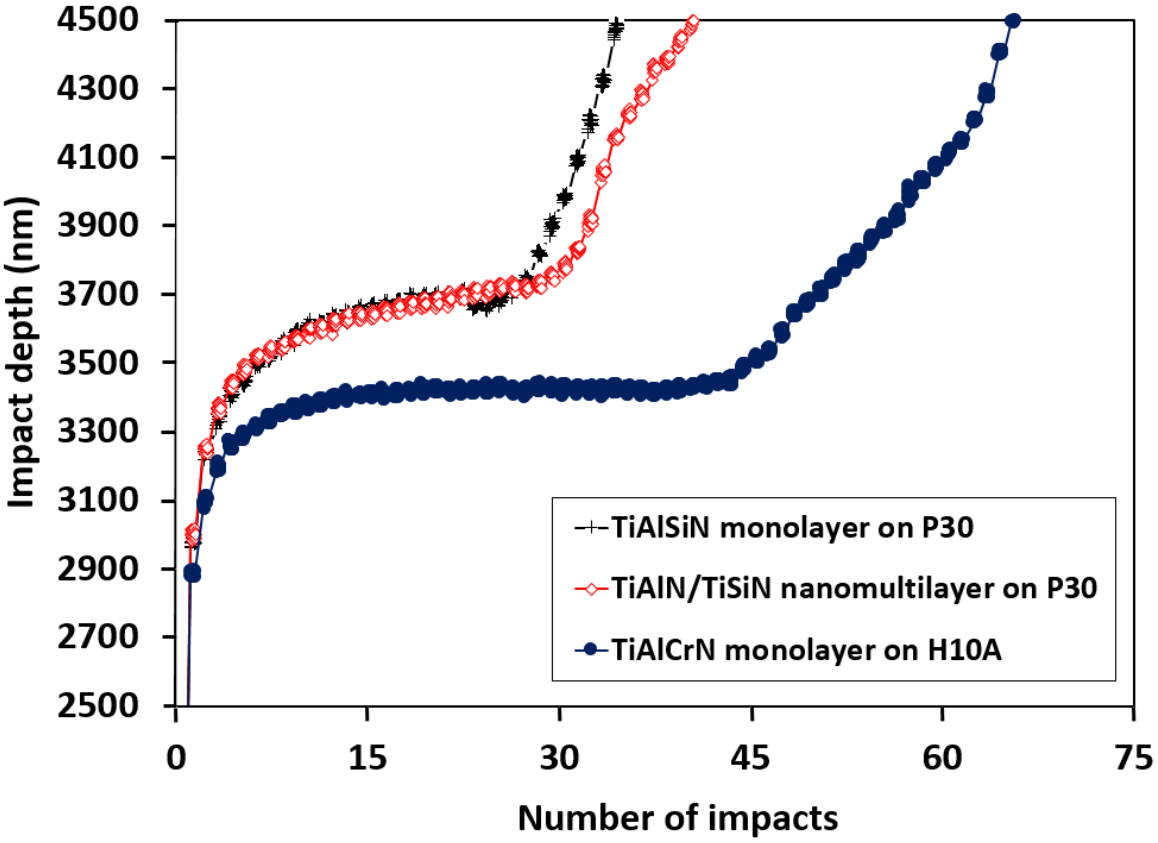
4500
4300
4100
3900
3700
3500
3300
3100
2900
2700
2500
Impact depth (nm)
0
15
30
45
60
75
Number of impacts
TiAlSiN monolayer on P30
TiAlN/TiSiN nanomultilayer on P30
TiAlCrN monolayer on H10A

2019-06-08

Elevated temperature micro-impact testing of TiAlSiN coatings produced by physical vapour deposition

Beake, Ben D.

Elsevier

Beake BD, Bird A, Isern L, et al., (2019) Elevated temperature micro-impact testing of TiAlSiN coatings produced by physical vapour deposition. Thin Solid Films, Volume 688, October 2019, Article number 137358

https://doi.org/10.1016/j.tsf.2019.06.008